Microprocessor Controlled Force Actuator

D. C. Zimmerman*
State University of New York at Buffalo, Buffalo, New York

G. C. Horner†
NASA Langley Research Center, Hampton, Virginia
and
D. J. Inman‡
State University of New York at Buffalo, Buffalo, New York

The mechanical and electrical design of a prototype force-actuator system for the vibration control of large space structures is reported. The force actuator is an electromagnetic system that produces a force by reacting against a proof mass. The actuator system is comprised of the actuator, two colocated sensors, an onboard digital microcontroller, and an onboard power amplifier. The dynamic characteristics of the actuator have been determined experimentally using digital Fourier analysis, and guidelines are suggested as to when they may be neglected in the implementation of the desired control law. Additionally, the results from an experiment are presented in which the actuator system is used to implement a rate-feedback control law to damp actively the transverse vibrations of a cantilevered beam. Finally, it is shown that the stability of the rate-feedback control law is not assured if the actuator dynamics are ignored during control-law implementation.

Introduction

FUTURE spacecraft and space structures are envisioned to be quite large by current standards. In consideration of the cost of transporting material into space, these spacecraft will most likely be lightweight, relatively flexible, and lightly damped. Thus, small disturbances may cause large amplitudes of vibration at low frequencies. Although the passive damping found in these structures may be an important dissipative mechanism,[1] the need to meet the stringent spacecraft performance criteria may require the use of active vibration control.

Numerous active control strategies have been proposed for the vibration control of large space structures (LSS).[2] To test and evaluate these active control strategies for spacecraft, ground tests must be performed to determine the practicality, safety, and actual performance. Before meaningful control studies can be performed, space-realizable actuators (SRA) must first be developed. Space-realizable actuators are those actuators which could conceivably work in space and therefore, most notably, are not attached to ground.

In recent years, there has been considerable research and development of SRA's.[3-19] These actuators can be categorized according to the type of load (torque, force, or strain) that they are capable of generating. They are summarized in this section.

A candidate torque-producing SRA is the gyrodamper.[3] A gyrodamper is made by configuring two control moment gyros as a scissored pair. By actively controlling the gimbal axes of the control moment gyros with torque motors, a net control torque can be applied to the structure. The reaction wheel[4-6] is an SRA which applies a control torque to the structure by reacting against a flywheel. As compared to the gyrodamper, the reaction wheel requires a larger wheel inertia to generate comparable levels of torque.[3] However, the reaction wheel is probably a simpler actuator to build for use in laboratory control experiments since a mechanism must be provided for in the gyrodamper for the two control moment gyros to gimbal in opposite directions.

The use of piezoelectric materials bonded to the structure, acting as both actuators and sensors, has recently received considerable attention.[7-9] As an actuator, the piezoelectric materials induce a local strain in the structure when a voltage field is applied across the material. This type of actuator has been demonstrated previously to be capable of controlling small amplitude vibrations of structures.[10,11]

A candidate force-producing SRA is the reaction jet.[12] Reaction jets have been used previously for rigid-body spacecraft maneuvers but have been used recently in the laboratory as actuators in structural vibration-control experiments.

A candidate force-producing SRA which is reported on in this paper is the proof-mass actuator. The proof-mass actuator is the translational equivalent of the reaction wheel in that it applies a force onto the structure by reacting against a translating proof mass.[13] The proof-mass actuator can only be used for vibration control since the finite travel limit of the proof mass does not allow the actuator to apply dc forces.

A variation of the proof-mass actuator is the pivoted proof-mass actuator.[13,14] This actuator can be configured to apply both control forces and torques. The pivoted proof-mass actuator consists of a mass at the end of a pivoted lever arm. The arm is permitted only small angle changes so that the mass undergoes a nearly linear motion. A variation of this actuator was developed[15] that allows the dynamic characteristics of the actuator to be changed by adjusting a passive spring and damper, which are located at the root of the pivoted lever arm.

The purpose of this paper is to describe the magnetic, electrical, and mechanical design of a linear drive proof-mass actuator. Additionally, the design of a power amplifier and a digital microcontroller for the actuator and a description of the collocated sensors are discussed. The dynamic characteristics of the actuator will be presented and shown to be an important consideration in control-law implementation. Finally, an active control experiment will demonstrate the capabilities of the actuator system.

Proof-Mass Actuator Description

The development of the proof-mass actuator was motivated by two separate aspects. First, to evaluate realistically control strategies for LSS, the actuators used should be space realizable. When the proof-mass actuator was developed, few, if any,

Received Oct. 8, 1986; revision received Feb. 16, 1987.

*Research Fellow, Department of Mechanical and Aerospace Engineering. Member AIAA.

†Aerospace Technologist, Structural Dynamics Branch.

‡Professor, Department of Mechanical and Aerospace Engineering. Member AIAA.

space-realizable actuators existed. Second, the design was motivated from the need to overcome some of the difficulties encountered in using conventional shakers as control actuators. Conventional shakers are often too heavy to be supported solely by the test structure, and thus, would require some type of suspension system. The requirement of a suspension system could conceivably reduce the number of possible actuator locations on the test structure and would make the relocation of actuators on the test structure a more difficult task. In addition, conventional shakers add considerable mass, stiffness, and damping[16] to the structure. If left uncompensated, the shakers could grossly alter the dynamic characteristics of the test structure, making the evaluation of the desired control law a formidable task. Therefore, a basic design goal for the actuator system was to have an actuator whose weight could be supported solely by the test structure and whose parasitic dynamic effects on the test structure would be minimal.

The actuator system is comprised of a movable proof mass, a fixed coil, two collocated sensors, a digital microcontroller, and a power amplifier. All of the components are mounted as a single unit (see Fig. 1). Power lines are the only external cables required by the actuator system to operate.

A schematic diagram of the proof-mass actuator is shown in Fig. 2. To increase the ratio of proof-mass weight to total actuator weight, a design[17] was chosen where the moving proof mass contains the permanent magnet flux source. In this configuration, the mass of the proof mass is 0.232 kg and the total actuator system mass is 0.998 kg. The magnetic flux is supplied by two toroidal samarium-cobalt magnets (item 13, Fig. 2). The use of two magnets, as opposed to one, does not increase the magnetic field available to the flux loop but does help to reduce the flux leakage at the annular gap. The remainder of the proof mass consists of the flux loop (item 12, Fig. 2) which is made of pure iron and a linear sleeve bearing (item 9, Fig. 2). The linear sleeve bearing allows the proof mass to translate freely one inch along a hardened steel shaft (item 8, Fig. 2). An aluminum outer case (item 10, Fig. 2) keeps the linear bearings clean and supports one end of the steel shaft. The total magnetic flux Φ_1 supplied by the permanent magnet to the flux loop is given as the product of B, the magnetic flux density of the magnets, and A, the area of contact between the magnets and the flux loop[17]

$$\Phi_1 = BA \tag{1}$$

The magnetic flux density of the magnets is given by the manufacturer to be 0.8 Weber/m^2, and the area of contact is calculated to be 1.91 cm^2. The total magnetic flux Φ_1 as calculated from Eq. (1) is 153 μWeber.

As shown in Fig. 2, the poles of the proof mass encompass the fixed coil (item 11, Fig. 2). The annular gap between the proof mass and the coil is large enough so that the proof mass is never in contact with the coil. The electromagnetic force F exerted on the proof mass, and therefore back onto the structure, is equal to the product of the magnetic flux density that is cut by the coil B_{gap}, the length of wire in the gap L_{gap}, and the current in the coil i,[17]

$$F = B_{gap} L_{gap} i \tag{2}$$

The magnetic flux density that is cut by the coil B_{gap} is equal to the total magnetic flux supplied to the gap Φ_2 divided by the average surface area of the two poles of the flux loop,[17]

$$B_{gap} = \Phi_2/(\pi D_1 w_p) \tag{3}$$

where D_1 is the average diameter of the two poles and w_p is the width of the poles.

The length of wire in the gap can be written as

$$L_{gap} = \pi D_2 n w_p \tag{4}$$

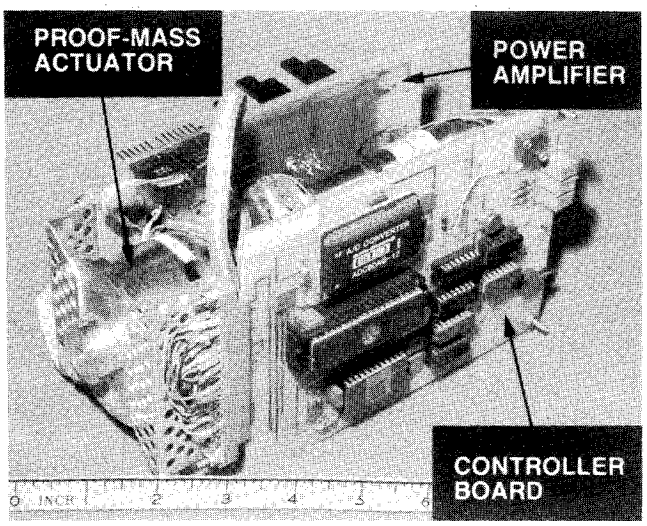

Fig. 1 Proof-mass actuator system.

where D_2 is the mean diameter of the coil and n is the number of turns of wire per meter of coil length.

Using Eqs. (2–4), the force F applied to the proof mass can be calculated from

$$F = \Phi_2(D_2/D_1)ni$$
$$= G_1 i \tag{5}$$

The length of the fixed coil is 3.175 cm and has ten layers of 26-gage copper wire, each layer consisting of 67 turns. Therefore, the coil has 21,124 turns of wire per meter of coil length.

To calculate a theoretical value of G_1 in Eq. (5), the assumption is made that there is no flux leakage at the annular gap and therefore the total available magnetic flux is cut by the coil. The value of Φ_2 in Eq. (5) is then equal to Φ_1 as calculated from Eq. (1). In addition, it is assumed that the average diameter of the two poles is approximately equal to the mean diameter of the coil. This approximation is as good as any attempt made to measure these two diameters directly. With these assumptions, the proportionality constant G_1 is calculated to be 3.23 N/A. In testing the actuator,[18,19] the proportionality constant was experimentally determined to be 2.75 N/A. The discrepancy between design calculations and the experimental findings can be attributed mainly to the assumption in Eq. (5) that the total available magnetic flux is cut by the coil.

Sensor Description

There are two collocated sensors in the actuator system (see Fig. 2). A dc servo-accelerometer is mounted on the outer case of the actuator. Since the outer case would be directly attached to the test structure, the accelerometer measures the local acceleration of the structure. The accelerometer has a linear output range of $\pm 20\ g$ and a resolution of 5 μg.

The other sensor attached to the actuator is a linear variable differential transformer (LVDT). An LVDT is an electromechanical transducer and consists of a core which slides freely inside a sleeve. The motion of the core relative to the sleeve produces an electrical signal proportional to the displacement. The core is attached to the proof mass and the sleeve is attached to the outer case (see Fig. 2). Therefore, the LVDT measures the relative position of the proof mass with respect to the structure, and therefore, to the fixed coil. The LVDT used has double magnetic shielding to prevent the magnets contained in the proof mass from affecting the sensor measurement. The bandwidth of the LVDT is given by the manufacturer to be 500 Hz.

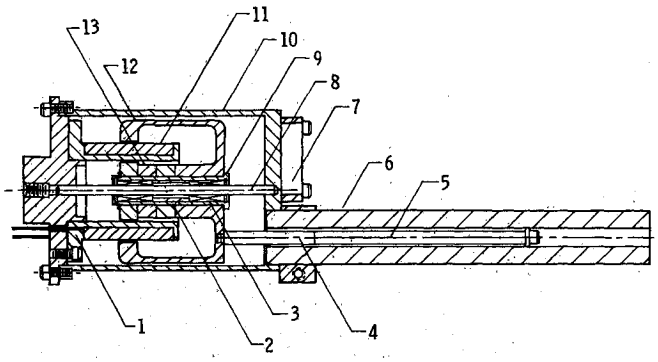

Fig. 2. Schematic and major parts list of proof-mass actuator.

Controller Board Description

The goal of the controller design was to provide the actuator system with a versatile controller that was small enough to be attached to the actuator. A digital-control system was chosen since control strategies may be changed by software, as opposed to the time-consuming hardware changes that would be necessary in an analog-control system.

The board has three analog-input channels, one analog-output channel, and two bidirectional digital lines. The LVDT and accelerometer outputs comprise two of the three analog inputs. The third analog channel is available for an auxiliary input signal. The three analog inputs are multiplexed to a 12-bit analog-to-digital convertor (A/D). The A/D has a 5 mV resolution and a conversion time of approximately 25 μs.

The digital output of the A/D is connected to an 8751 microcontroller,[20] which is an erasable-programmable read-only memory (EPROM) 8-bit microcontroller. The 8751 microcontroller has an 8-bit CPU, a Boolean processor, an oscillator and clock circuitry, 32 TTL I/O lines, 128 bytes of random access memory (RAM), 4K of program memory (EPROM), and two 16-bit timer/counters.

An 8751 microcontroller output port drives a 12-bit digital-to-analog converter (D/A). The D/A has an output resolution of 5 mV. The analog output of the D/A is connected to the power amplifier input which is described in the next section.

The 12-bit A/D and D/A comprise 24 of the 32 available TTL I/O lines of the 8751 microcontroller. Of the eight remaining lines, seven are currently used. The A/D multiplex address circuit requires two TTL lines. An additional two lines are used for handshaking with the A/D; one for issuing a start of conversion command and the other for reading an end of conversion. Another TTL line is used to operate an electronic switch that connects the D/A output to the power amplifier. This switch was included so that the D/A was not connected to the amplifier on a power-up operation (in which the D/A outputs -10 V). The last two TTL lines are sent off card to an optional remote site controller. The state of one of these lines is reflected by a LED. These two lines were included so that the overall operations of the actuator could be monitored and controlled. For example, one of the lines could be used to switch the processor between execution of two different control programs that simultaneously reside in EPROM.

Power Amplifier Description

A voltage-controlled power amplifier is used to drive the coil of the actuator. The amplifier takes the low power, high-impedance D/A output command and creates a high power, low-impedance output command to match the 8-Ω load of the fixed coil. The power amplifier maintains a given current in the coil for a given voltage input. The ratio of the voltage input to the current output can be modified by adjusting a variable resistor located on the amplifier board. This gain (G_2 in the next section) is presently set to 0.1 A/V to avoid overheating the fixed coil. The bandwidth of the amplifier is greater than 10 kHz, which is well above the frequency range of interest for LSS.

Description of Actuator Dynamics

Many researchers have developed various control laws to reduce the vibrations of LSS. These control laws have generally been based solely on the dynamic properties of the structure to be controlled. The importance of actuator (and sensor) dynamics has received recent attention in the literature.[21–23] It has been shown that actuator dynamics, if not properly treated, may cause an otherwise stable system to become unstable.[21] Another approach taken has been to derive control laws ignoring actuator dynamics, but the effects of actuator dynamics are then later evaluated.[22] Recently, it has been shown that an integrated actuator dynamics/control law design approach can greatly improve the control system performance.[23]

The dynamic characteristics of the proof-mass actuator were determined so that they may be included in future control work. Additionally, the dynamic testing was used to determine the physical limitations of the actuator. A detailed description of the dynamic modeling and testing is reported in Refs. 18 and 19. For the sake of completeness, a brief summary of the findings is included herein.

The motion of the proof mass is controlled by the force of the electromagnetic field which is created when there is a current in the fixed coil. Since the electromagnetic force can barely lift the weight of the proof mass, the actuator is most effective when it is aligned in the horizontal plane. However, in laboratory experiments, the actuator can never be aligned exactly with the horizontal reference since it is mounted on a moving structural model. Therefore, a centering force is needed to overcome the force component due to gravity which would cause the proof mass to slide to one end and impact the outer case. A centering force proportional to the displacement of the proof mass from the center of the fixed coil is created in software by feeding back the LVDT signal multiplied by an appropriate constant. Additionally, the relative motion of the proof mass with respect to the coil is damped. The damping is caused by the back-emf in the coil which is induced when there is relative motion of the coil with respect to the proof mass.[18,19] The damping effect of the back-emf can be modified by the addition in software of a differentiated LVDT feedback loop.

Figure 3 shows a model of the actuator attached to a generic structure using mechanical analogies for the electronic forces. When attached to a structure, the actuator can be modeled as a single degree of freedom untuned vibration absorber with a force generator acting between the structure and absorber mass. In Fig. 3, M_s is the mass of the structure (including the parasitic mass of the actuator) and K_s is the stiffness of the structure. The actuator dynamics are modeled as m_p, the mass of the proof mass, k_p, the stiffness of the electronic centering force, and c_p, the effect of the back-emf damper. The addition of the desired control law can be modeled as f_g, a force generator which applies equal but opposite forces onto the structure and the proof mass.

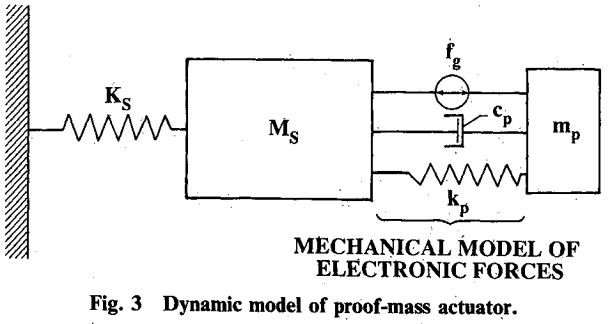

Fig. 3 Dynamic model of proof-mass actuator.

A typical frequency-response measurement of the total actuator force output (spring, damper, and force generator reactions) to voltage command to the force generator is shown in Figs. 4a and 4b. In these measurements,[18,19] the mass of the structure M_s was locked (not free to move). The measurements, therefore, reflect solely the dynamics of the proof-mass actuator.

To obtain the actuators' frequency response, the force output of the actuator was measured as a function of the voltage command to the force generator. The voltage command was a random signal with a Gaussian distribution. Several frequency-response measurements were made and averaged to minimize the effect of measurement noise on the calculation of the frequency response. The transfer function for the actuator dynamics can be obtained by writing the equation of motion for the proof mass, utilizing both the definition of G_2 and Eq. (5)

$$F(s) = G_1 G_2 V_t(s) = m_p s^2 X(s) \tag{6}$$

where F is the total force applied onto the proof mass (and therefore back onto the structure), G_1 is the electromagnetic gain (either calculated from Eq. (5) or determined experimentally), G_2 is the power amplifier gain (0.1 A/V), X is the absolute position of the proof mass, and s is the Laplace operator. The total voltage applied across the coil V_t can be written as

$$V_t = V - V_{c_p} - V_{k_p} = V - c_p s X(s) - k_p X(s) \tag{7}$$

where V is the voltage command to the force generator, V_{c_p} the voltage drop corresponding to the back-emf damper, and V_{k_p} the voltage command corresponding to the electronic centering force. Substituting Eq. (7) into Eq. (6) and rearranging gives

$$\frac{X(s)}{V(s)} = \frac{G_1 G_2}{m_p s^2 + G_1 G_2 c_p s + G_1 G_2 k_p} \tag{8}$$

Multiplying both sides of Eq. (8) by $m_p s^2$, and recognizing that $m_p s^2 X(s)$ is just the total force applied onto the proof mass (and the structure), the transfer function of the total actuator force output to voltage command to the force generator can be written as

$$\frac{F(s)}{V(s)} = \frac{G_1 G_2 m_p s^2}{m_p s^2 + G_1 G_2 c_p s + G_1 G_2 k_p} \tag{9}$$

The electronic centering force stiffness k_p is determined by the sensitivity of the LVDT (393.7 V/m) and the user programmable gain contained in the 8751 control program. The back-emf damping constant of the actuator was determined experimentally to be 12.72 V-s/m.[18,19]

Theoretically, the values of c_p and G_1 should be numerically equal when expressed in equivalent units. The discrepancies can be attributed to the theoretical assumptions made (such as zero flux leakage) in stating that c_p and G_1 should be equal and in the experimental determination of the constant c_p (the value for G_1 is accurate). The constant c_p was found by identifying the damping present in the actuator dynamics.[18,19] The measurement of damping in a system can be quite inaccurate,[24] and this could cause substantial error in the calculation of c_p. In Figs. 4a and 4b, the solid lines show the experimentally measured frequency-response function. The ⊙ points on the figure were determined from Eq. (9) using the experimentally determined constants. The value of k_p for this particular measurement was 449.7 V/m.

The dynamics of the actuator can be seen to be just that of a second-order high pass filter whose characteristics are shaped by the spring and damper rates. The break frequency of the high pass filter is defined to be the frequency at which the phase

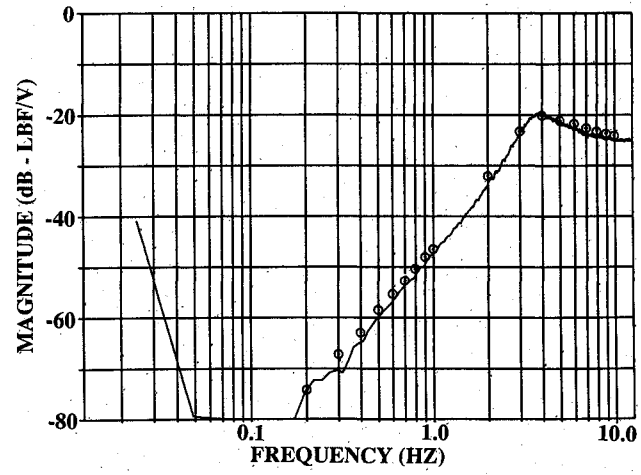

Fig. 4a Proof-mass actuator frequency response—magnitude of force output vs voltage command.

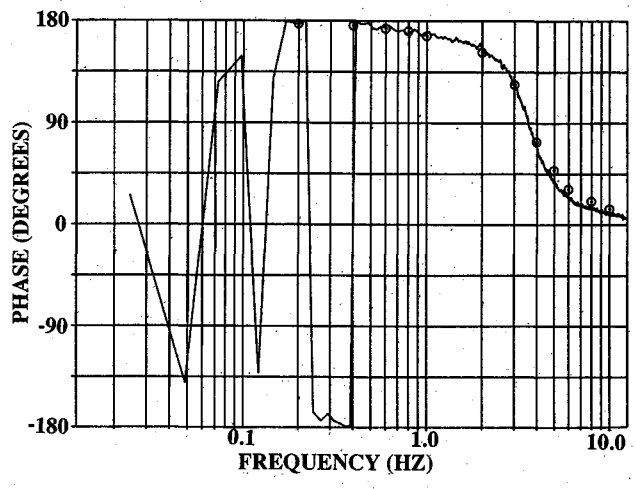

Fig. 4b Proof-mass actuator frequency response—phase of force output vs voltage command.

plot goes through 90 deg and the magnitude plot breaks flat from a 40 dB/decade rise. Additionally, one can define an operational frequency ω_{op} above which the magnitude of the frequency-response function is independent of frequency and there is approximately zero phase difference between the force output of the actuator and voltage command to the force generator. Therefore, above ω_{op}, the actuator can be viewed as behaving like an ideal force actuator because the force output directly follows the voltage command to the force generator. As the frequency of the voltage command to the force generator tends from ω_{op} to dc, the force output begins to lag the voltage command and the magnitude of the force output begins to decrease. Therefore, if the desired control law (voltage command to the force generator) has frequencies below ω_{op}, the dynamics of the actuator can become important during control-law implementation.

The frequency ω_{op} is dependent upon many actuator parameters, including the spring feedback rate and the weight and allowable stroke length of the proof mass. Although the back-emf damping rate certainly affects the frequency response of the actuator, changes in the damping rate have counteracting effects on the magnitude and phase responses such that ω_{op} is not affected. The only variable that affects ω_{op} that can be easily modified in the current configuration is the spring feedback rate. Lowering the spring feedback rate has the effect of lowering ω_{op}.

When the structural mass is free to move, the dynamics of the actuator and structure become coupled. The effect of coupling on the force output of the actuator must be investigated

for each particular structural control problem of interest.[23] If the amplitude of structural displacements and velocities are small in comparison to the proof masses' displacement and velocity, the effect of coupling on the force output of the actuator is minimal. A further practical consideration in using the actuator is the finite travel limit of the proof mass. The proof mass has a travel limit of one inch with respect to the structure. The total force applied to the structure (and thus to the mass) must be constrained such that the force does not cause the relative motion of the proof mass to exceed the travel limit. The travel of the proof mass with respect to the structure is dependent upon the relative spring and damping rates, the command to the force generator, and the motion of the structure. Although this actuator has been used successfully in control experiments, the interdependence of these factors certainly warrants further investigation.

Control-Law Implementation and Experimental Demonstration

An active control experiment was performed to show the capabilities of the actuator system and also point out some considerations that must be made when implementing a control law. The experimental apparatus consists of a cantilevered beam with the actuator system attached at the tip. In addition, there is an accelerometer mounted at the tip which is used for monitoring the vibration of the beam. The control law used is a local rate-feedback law which effectively damps the transverse vibrations of the beam.

To implement the control law, an 8751 assembly language program was written that calculates the local velocity of the beam at the tip by integrating the actuator-borne dc servo-accelerometer signal using a first-order Euler approximation. The local velocity is then multiplied by an appropriate constant to obtain the desired rate-feedback control law. In addition, the control program creates the centering spring by feeding back the LVDT signal multiplied by an appropriate constant.

In integrating the accelerometer signal to obtain the structures velocity, two important considerations must be made. First, the dc bias of the accelerometer output must be made to be as small as possible or the dc bias will integrate to infinity as time goes to infinity. In practical terms, the dc bias must be made to be as close to zero as possible so that the effects of the bias are not noticeable over a reasonable length of time. In the test set-up, the dc bias level was adjusted to be less than the resolution of the A/D converter. A second consideration in performing the integration is that the 8751 assembly language only supports integer operations. Because Δt (the sample period of the control program) in the Euler integrator is much smaller than unity, the multiplication by Δt is replaced by an integer division by the integer number closest to $1/\Delta t$. A quasifloating point integer integration (QFPII) algorithm was developed to overcome the truncation errors that occur due to integer division. The QFPII method utilizes the remainder of the integer division to improve the instantaneous velocity approximation. It is called a quasifloating point algorithm because the output command of the D/A to the actuator power amplifier would be exactly the same as if the velocity calculation had been performed on a floating point machine. Additionally, a double precision macroassembly language was written and implemented to further improve the accuracy of the velocity calculation.

Since the rate-feedback control law will have the same frequency spectra as the beam, the centering spring constant is set such that the operational frequency (and therefore the break frequency) of the actuator system is lower than the first bending mode of the beam. Additionally, the input disturbance to the beam during testing must be limited so that the proof masses' displacement and velocity are greater than those of the structure and that the displacements do not exceed the stroke-length limit. By doing this, the effects of actuator dynamics on the desired control law can essentially be ignored. These are very important considerations that should not be overlooked in any control experiment.

A photograph of the experimental set-up is shown in Fig. 5. The test structure is 0.654 m long and is made of a quasi-isotropic composite material.[25] The sample period Δt is the time elapsed in looping through the 8751 control program once. For this experiment, the sample period was 7.6×10^{-4} s. To demonstrate the effects of the rate-feedback control law, the uncontrolled structure is defined to be the cantilevered beam with the parasitic mass of the actuator located at the tip, i.e., M_s and K_s of Fig. 3. The controlled structure is then defined to be the uncontrolled structure along with the active control law, i.e., m_p, c_p, k_p, and f_g of Fig. 3. In measuring the frequency-response function of the uncontrolled structure, the proof mass was removed from the actuator.

The magnitude of the inertance frequency-response function of the uncontrolled and controlled structure are shown in Figs. 6a and 6b. The frequency-response functions were obtained by impacting the test structure with a calibrated force hammer (in the same location for both the uncontrolled and controlled cases) and measuring both the force input–time history and the structures' free-decay response. The structures' free decay was measured using the independent accelerometer mounted at the tip of the beam. The actuator-borne accelerometer was not used as a measurement sensor to avoid possible corruption of the controller input signal with line noise. A standard force window was applied to the force measurement to minimize the effects of noise. No response window was applied to the free-decay measurement because the standard exponential window manifests itself in the measured frequency response as an artificial increase in modal damping. A total of six frequency-response functions for each case were made and averaged to further minimize the effects of measurement noise. Additionally, the free-decay tip acceleration of the uncontrolled and controlled structure, subject to equivalent initial impacts (as measured by the energy content of the hit) are shown in Figs. 7a and 7b. The magnitude of the impact was such that for the controlled structure, the full stroke length of the actuator was utilized.

In measuring the inertance frequency response of the uncontrolled structure, it should be noted that the structure was very lightly damped. The impact force level required to maintain a reasonable signal to noise ratio was such that the free-decay vibration of the structure persisted for a time period longer than the time window of the frequency analyzer. This can result in a phenomena known as leakage,[26] as is evidenced in the frequency-response measurement between structural modes one and two. To minimize the effects of leakage, an exponential weighting window can be applied to the free-decay response to artificially damp the response. This was done and the results verify that the spikes in the measured frequency response between modes one and two of Fig. 6a were caused by leakage.

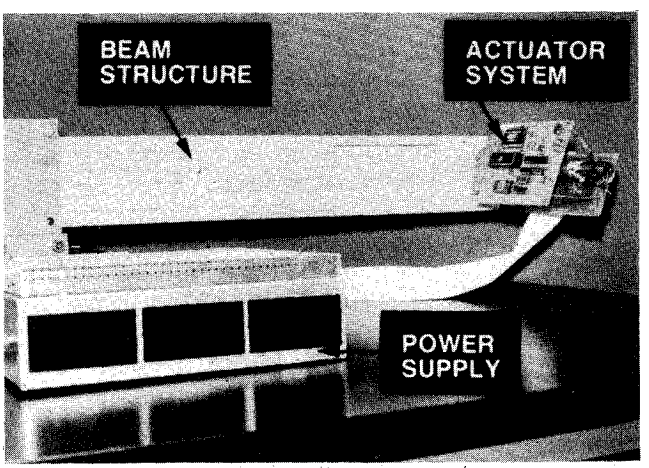

Fig. 5 Cantilevered beam/proof-mass actuator—controlled structure.

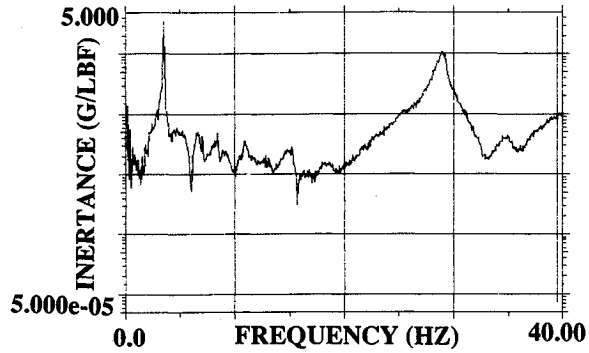

Fig. 6a Inertance frequency response function—uncontrolled structure.

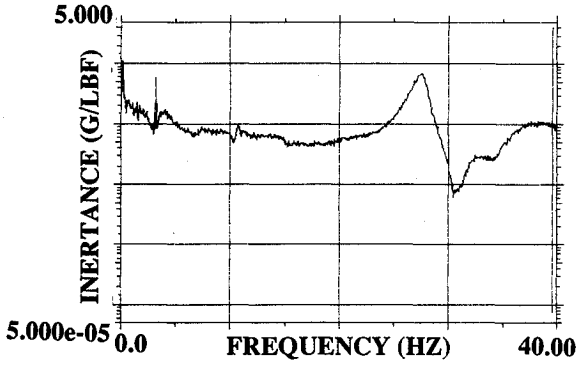

Fig. 6b Inertance frequency response function—controlled structure.

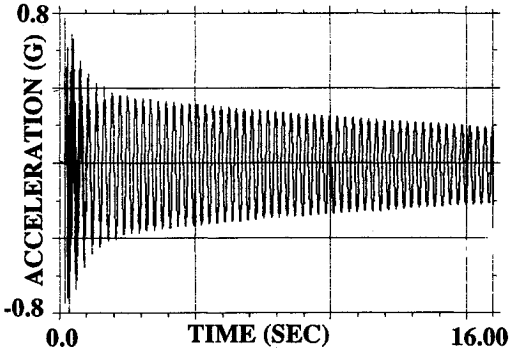

Fig. 7a Free-decay tip acceleration—uncontrolled structure.

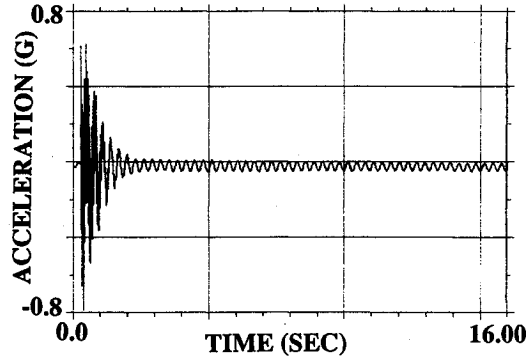

Fig. 7b Free-decay tip acceleration—controlled structure.

To evaluate the effects of the rate-feedback control law, a single degree of freedom circle-fit method[26] was used to extract the modal parameters (natural frequencies and damping rates) of the uncontrolled and controlled structure. The first mode damping rates were also approximated using the logarithmic decrement technique.[27]

Using the circle-fit method, the first two modes of vibration of the uncontrolled structure were identified at 3.49 Hz and 28.91 Hz with damping rates of 0.2 and 1.0%, respectively. The logarithmic decrement technique gave evidence of an amplitude dependent nonlinear first mode damping rate. An estimate of the linear first mode damping rate was determined to be 0.4%.

The circle-fit method identified the first three modes of the controlled structure, a spring-mass actuator dominant mode and the first two beam modes at 3.19, 4.16, and 27.55 Hz, respectively. The first and second beam mode damping rates were estimated to be 7.3% and 1.3%, respectively. The logarithmic decrement technique estimated the first mode damping rate to be 9.2%.

The estimates of damping show that the rate-feedback control law greatly increases the damping rate of the first mode, while having a moderate effect on the second mode of vibration. This was expected since the actuator location was near the antinode of the first mode and the node of the second mode of the structure.[5]

Figure 7b shows that the vibrations of the controlled structure do not damp out completely but exhibit a lightly damped oscillation. It is felt that this is caused by a nonlinear quantization error associated with the D/A and A/D of the digital controller in the control-law implementation[28] and the inherent actuator dynamics. At high levels of structural vibration (and therefore high levels of acceleration measurement), the nonlinear effects of quantization on the accuracy of the calculation of the structures velocity is minimal. Therefore, the calculation and implementation of the rate-feedback control law is linear. However, as the structural vibrations damp to lower levels, the nonlinear effect of quantization greatly influences the accuracy of the calculation of the structures velocity. Therefore, at low levels of structural vibration, the nonlinear quantization errors greatly affect the calculation and implementation of the rate-feedback control law. This nonlinearity introduced into the control law (which essentially now is a nonlinear viscous damper) causes the structure to exhibit a lightly damped oscillation.

Of notable interest is that the frequency-response functions show that the first beam mode of the controlled structure (4.16 Hz) is actually higher than the first beam mode of the uncontrolled structure (3.49 Hz). This result is a direct consequence of the first monotonicity principle[29] if the affects of the active controller are viewed as just a change in the boundary conditions between the uncontrolled and controlled structure.

Although the actuator dynamics have been ignored in this experiment, it is of considerable interest to examine the case where the centering spring constant cannot be set low enough (because of actuator misalignment and/or stroke-length limitations) such that the break frequency of the actuator is higher than some of the beam frequencies. In this case, the frequency spectra of the control law has frequencies both below and above the break frequency. Because the phase characteristics of the actuator, the rate-feedback control law is unstable. If the beam modes are grouped into those which have frequencies above and those which have frequencies below the actuator break frequency, it can be shown that the stability of the two groups are mutually exclusive.

Summary

The design of a candidate force-actuator system for the vibration control of large space structures has been reported. The actuator system is comprised of the proof-mass actuator, the colocated sensors, an onboard digital microcontroller, and an onboard power amplifier. The actuator is space realizable in that it is not required to be attached to ground. The actuator applies a force to the structure by reacting against a proof mass. The dynamic characteristics of the actuator were determined and a linear, time-invariant mathematical model formulated. The paper provides a model of the actuator dynamics for

a practical on-board control actuator for future use in theoretical and experimental studies in the area of control-structure interaction.

An experimental demonstration of the actuator system shows that the effects of actuator dynamics and digital implementation of the desired control law are important considerations. The experiment demonstrated that the actuator system was able to significantly damp the transverse vibrations of the cantilevered beam.

Acknowledgments

This work was supported by NASA under the Graduate Student Researchers Program, Grant NGT 33183801; and in part by National Science Foundation, Grant MEA-835-1807; and Air Force Office of Scientific Research, Grant AFOSR 85-0220. The research was conducted at the Structural Dynamics Branch of NASA Langley Research Center and the Mechanical Systems Laboratory of the State University of New York at Buffalo.

References

[1]Ashley, H., "On Passive Damping Mechanisms in Large Space Structures," *Journal of Spacecraft and Rockets*, Vol. 21, No. 5, Sept.–Oct. 1984, pp. 448–455.

[2]Balas, M. J., "Trends in Large Space Structure Control Theory: Fondest Hopes, Wildest Dreams," *IEEE Transactions on Automated Controls*, Vol. AC-27, No. 3, June 1982, pp. 522–535.

[3]Aubrun, J. N. and Margulies, G., "Gyrodampers for Large Space Structures," NASA CR-NAS1-14887-Task 6, Feb. 1979.

[4]Wernli, A., "Minimization of Reaction Wheel Momentum Storage with Magnetic Torquers," *The Journal of Astronautical Sciences*, Vol. 26, No. 3, July–Sept., 1978, pp. 257–278.

[5]Mills, R. A., "Active Vibration Control of a Cantilevered Beam: A Study of Control Actuators," *34th Congress of the International Astronautical Federation*, Budapest, Hungary, Oct. 1983.

[6]Montgomery, R. C., "Experiments in Structural Dynamics and Control Using a Grid," *Proceedings of the Workshop on Identification and Control of Flexible Space Structures*, JPL publication 85-29, Vol. 1, April 1985.

[7]Hanugud, S., Obal, M. W., Meyyappa, M., "Electronic Damping Techniques and Active Vibration Control," *Proceedings of the AIAA/ASME/ASCE/AHS 26th Structures, Structural Dynamics, and Materials Conference*, Orlando, FL, April 1985, Paper No. 85-0752.

[8]Crawley, E. F. and DeLuis, J., "Use of Piezo-Ceramics as Distributed Actuators in Large Space Structures," *Proceedings of the AIAA/ASME/ASCE/AHS 26th Structures, Structural Dynamics, and Materials Conference*, Orlando, FL, April 1985, Paper No. 85-0626.

[9]Bailey, T. and Hubbard, J. E. Jr., "Distributed Piezoelectric-Polymer Active Vibration Control of a Cantilever Beam," *Journal of Guidance, Control, and Dynamics*, Vol. 8, No. 5, Sept.–Oct. 1985, pp. 603–611.

[10]Olsen, H. F., "Electronic Control of Mechanical Noise, Vibration, and Reverberation," *Journal of the Acoustical Society of America*, Vol. 28, No. 5, Sept., 1956, pp. 966–972.

[11]Forward, R. L., "Electronic Damping of Orthogonal Bending Modes in a Cylindrical Mast—Experiment," *Journal of Spacecraft and Rockets*, Vol. 18, No. 1, Jan.–Feb., 1981, pp. 11–17.

[12]Floyd, M. A. and Van der Velde, W. E., "Verification of RCS Controller Methods for Flexible Spacecraft," Volume II, Report No. AFRPL-TR-84-092-V2, Dec. 1984.

[13]Aubrun, J. N. and Margulies, G., "Low Authority Control Synthesis for Large Space Structures," NASA CR-NAS1-14887, May 1982.

[14]Miller, D. W., "Dynamic Profile of a Prototype Pivoted Proof-Mass Actuator," MIT SSL Report No. 29-81, Aug. 1981.

[15]Miller, D. W., Crawley, E. F., and Ward, B. A., "Inertial Actuator Design for Maximum Passive and Active Energy Dissipation in Flexible Space Structures," *Proceedings of the AIAA/ASME/ASCE/AHS 26th Structures, Structural Dynamics, and Materials Conference*, Orlando, FL, April 1985, Paper No. 85-0777.

[16]Montgomery, R. C., Horner, G. C., and Cole, S. R., "Experimental Research on Structural Dynamics and Control," *Proceedings of the Third VPI&SU/AIAA Symposium on Dynamics and Control of Large Flexible Spacecraft*, Blacksburg, VA, 1981, pp. 365–378.

[17]Pilkey, W. D. and Haviland, J. K., "Large Space Structure Damping—Final Report," University of Virginia Report No. UVA/5-28201/MAE 83/101, Feb. 1983.

[18]Zimmerman, D. C., "Dynamic Characterization and Microprocessor Control of the NASA/UVA Proof Mass Actuator," M. S. Thesis, University of Buffalo, NY, June 1984.

[19]Zimmerman, D. C., Inman, D. J., and Horner, G. C., "Dynamic Characterization and Microprocessor Control of the NASA/UVA/UB Proof-Mass Actuator," *Proceedings of the 25th AIAA/ASME/ASCE/AHS Structures, Structural Dynamics and Materials Conference*, Palm Springs, CA, May 1984, Paper No. 84-1077.

[20]Microcontroller Handbook, Intel Corp., 1984, pp. 11-25–11-40.

[21]Caughey, T. K. and Goh, C. J., "Vibration Suppression in Large Space Structures," *Proceedings of the Workshop on Applications of Distributed System Theory to the Control of Large Space Structures*, April 1983, pp. 119–142.

[22]Kosut, R. L. and Salzwedal, H., "Stability and Robustness of Control Systems for Large Space Structures," *Proceedings of the Third VPI&SU/AIAA Symposium on the Dynamics and Control of Large Flexible Spacecraft*, Blacksburg, VA, 1981, pp. 343–364.

[23]Harokopos, E. G. and Mayne, R. W., "Motor Characteristics in the Control of a Compliant Load," *Journal of Guidance, Control, and Dynamics*, Vol. 9, No. 1, Jan.–Feb. 1986, pp. 113–118.

[24]Ewins, D. J., *Modal Testing: Theory and Practice*, Research Studies Press Ltd., Letchworth, England, 1986.

[25]Wilson, M. L. and Miserentino, R., "Protrusion Process Development for Long Space Boom Models," *Proceedings of the 41st Annual Conference of the Society of Plastics Industry*, Atlanta, GA, Jan. 27, 1986, paper 6-D.

[26]SDRC Modal Analysis User Manual 9.0, General Electric CAE International, Milford, OH, 1985, pp. 6-23–6-31.

[27]Meirovitch, L., *Elements of Vibration Analysis*, McGraw-Hill, New York, 1975.

[28]Kuo, B. C., *Digital Control Systems*, Holt, Rinehart and Winston, Inc., New York, 1980.

[29]Weinberger, H. F., "Variational Methods for Eigenvalue Approximation," *Regional Conference Series in Applied Mathematics*, SIAM, 1974, pp. 58–62.